Geophysical Journal International

Geophys. J. Int. (2010) doi: 10.1111/j.1365-246X.2010.04596.x

A dynamo cascade interpretation of the geomagnetic dipole decrease

Hagay Amit[1] and Peter Olson[2]

[1] *CNRS, Université de Nantes, Nantes Atlantiques Universités, UMR CNRS* 6112, *Laboratoire de Planétologie et de Géodynamique,* 2 *rue de la Houssinière,* F-44000 *Nantes, France. E-mail: Hagay.Amit@univ-nantes.fr*

[2] *Department of Earth and Planetary Sciences, Johns Hopkins University, Baltimore,* MD 21218, *USA*

Accepted 2010 March 11. Received 2010 March 11; in original form 2009 November 13

SUMMARY

We propose a spectral transfer model for the secular variation of the geomagnetic core field to explain the simultaneous decrease in dipole field intensity and the increase in non-dipole field intensity from 1840 to the present in terms of a dynamo cascade process. The main assumption of this model is that magnetic energy is transferred between adjacent spherical harmonic degrees in the Mauersberger–Lowes spectrum of the geomagnetic field. The key parameters are a set of coefficients γ_n that indicate the rate and direction of magnetic energy transfer through the spectrum. Applying the spectral transfer model to the historical period, we find that the quadrupole family of the core field can be characterized by a persistent inverse magnetic energy cascade from higher towards lower spherical harmonics. In the dipole family of the core field, we find cascade behaviour generally from lower to higher spherical harmonics, consistent with axial dipole decrease, but with a high level of time variability that correlates with variations in the dipole family intensity. During time intervals when the dipole family intensity rapidly decreases, energy appears to cascade towards higher spherical harmonics, beyond the limit of the observable part of the core field spectrum. During time intervals when the dipole family intensity is nearly constant, a more limited forward cascade appears to trap energy at intermediate spherical harmonics. Similar fluctuations in the rate and direction of spectral transfer are also seen in the Mauersberger–Lowes spectrum of a numerical dynamo model during a dipole decrease event that led to a polarity excursion. We discuss the possibility of this scenario for the current geomagnetic dipole decrease.

Key words: Dynamo: theories and simulations; Geomagnetic excursions; Rapid time variations.

1 INTRODUCTION

During the historical period, the shape of the low degree part of the geomagnetic field spectrum has rapidly changed with time. Since the advent of geomagnetic field intensity measurements about 170 yr ago, the geomagnetic dipole moment has been losing intensity, while at the same time the non-dipole part of the core field has been gaining intensity. According to the historical *gufm1* field model (Jackson *et al.* 2000), the geomagnetic dipole moment has dropped from 8.50×10^{22} Am^2 in 1840 to 7.84×10^{22} Am^2 in 1990, and similarly, its dominant axial component has decreased from 8.33×10^{22} Am^2 in 1840 to 7.70×10^{22} Am^2 in 1990. The rate of change of the axial dipole moment in 1990 was -4.38×10^4 Am^2 yr^{-1}, compared to the average rate of -4.22×10^4 Am^2 yr^{-1} over the 150-yr period. Recent geomagnetic field models based on satellite data show that the historical dipole decrease continues to the present-day. According to the *xCHAOS* field model (Olsen & Mandea 2008), the 2009 dipole moment was 7.75×10^{22} Am^2, its axial component was 7.63×10^{22} Am^2, and its current rate of change is -4.92×10^4 Am^2 yr^{-1}, indicating that the dipole decrease has recently accelerated.

Fig. 1 shows time-series of the rms field intensity, rms dipole intensity, rms axial dipole intensity, and rms non-dipole field intensity on the core–mantle boundary (CMB) from 1840 to present. The period 1840–1990 is covered by model *gufm1* from which we expanded until spherical harmonic degree $n_{\max} = 8$, while the period 1999–2009 is represented by model *xCHAOS* until $n_{\max} = 14$. The mismatch between the rms field intensities in the two models reflects different regularization assumptions and different levels of harmonic truncation due to the greater quality and time resolution of the modern data. While the dipole field decreases monotonically in both models, the non-dipole field has the opposite trend, substantially increasing with time. Overall, the rms intensity (Verosub & Cox 1971; Benton & Alldredge 1987) and the average absolute value of the radial component (Benton & Voorhies 1987) of the core field have changed relatively little during the historical period; if anything, they have increased very slightly, although this may be an artefact of improved resolution of the core field with time.

Were the current trends to persist, the axial dipole would hypothetically vanish in about 1600 yr time. However, the dipole variation has not been uniform in the past. Evidence suggests that the

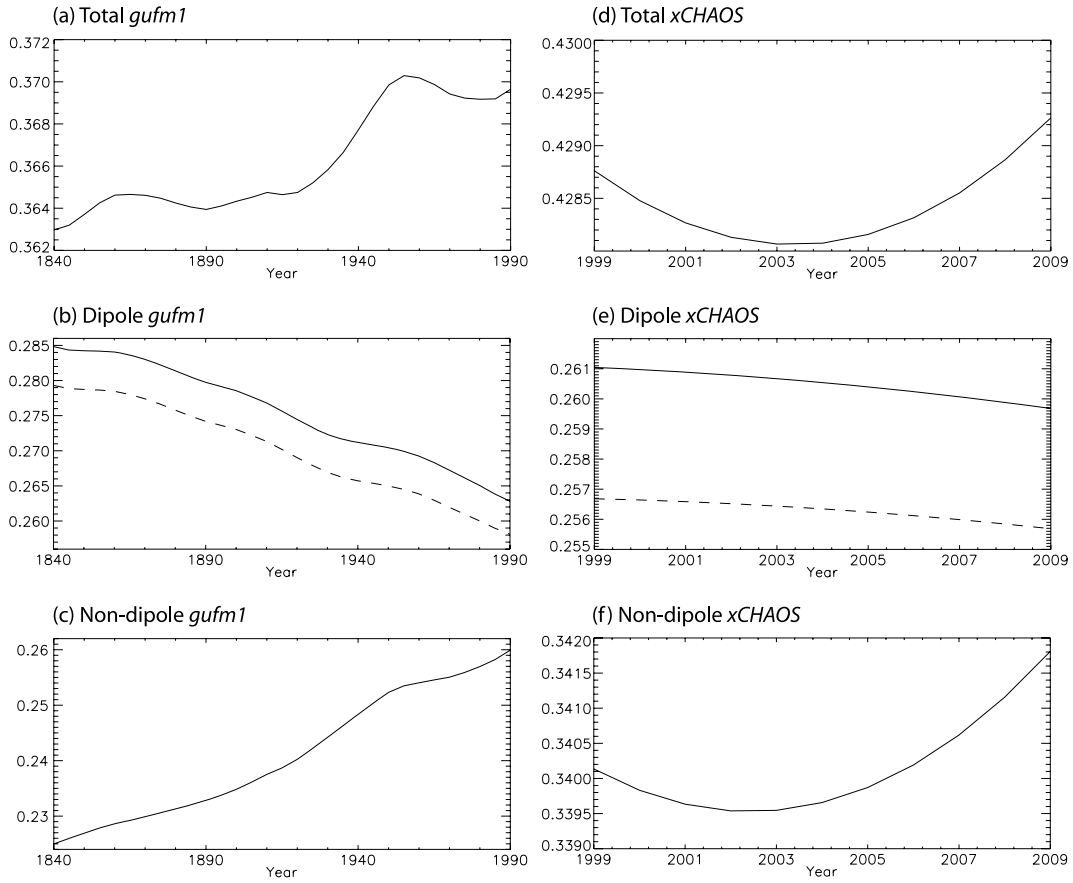

Figure 1. Time-series of the rms core field intensities: (a) total field $B_{\rm rms}$; (b) dipole $B_{\rm rms}(n = 1)$ and axial dipole $B_{\rm rms}(n = 1, m = 0)$; and (c) non-dipole $B_{\rm rms}(n > 1)$, all from model *gufm1* (Jackson *et al.* 2000) to spherical harmonic degree $n_{\rm max} = 8$ for the period 1840–1990, and similarly (d)-(f) from model *xCHAOS* (Olsen & Mandea 2008) to $n_{\rm max} = 14$ for the period 1999–2009. All intensities are in *mT* at the core–mantle boundary. In (b) and (e) the solid curve is the full dipole intensity and the dashed curve is the axial dipole intensity. 1 Am^2 is equivalent to $3.87 \cdot 10^{-25}$ mT for the geomagnetic g_1^0 Gauss coefficient, or to $2.74 \cdot 10^{-24}$ mT for the corresponding rms field.

dipole decrease during the 250 yr prior to 1840 was significantly slower than today (Gubbins *et al.* 2006), possibly remaining constant (Finlay 2008) during that time. According to the archaeomagnetic core field model *CALS7K.2* (Korte & Constable 2005), the current episode of dipole decrease began within the past 1 kyr and followed a period of about 2 kyr when the dipole intensity fluctuated. Less is known about the non-dipole core field during that time, but the irregular dipole variations over the past 3 kyr, and moreover, the opposing trends of the dipole and non-dipole parts over the past 150 yr, are the primary evidence that the shape of the geomagnetic spectrum undergoes rapid changes.

There are a variety of dynamo mechanisms that could drive the dipole and non-dipole fields in opposite directions. One possibility is that magnetic diffusion is preferentially weakening the dipole field by decay of its higher modes (Moffatt 1978) or by expulsion of reversed dipolar field from the core (Bloxham 1986), while at the same time, dynamo processes are strengthening the non-dipole field. Another possibility is that advection by fluid motions in the outer core is distorting the pattern of the field on the CMB, and thereby directly transferring magnetic energy from the dipole part to the non-dipole part of the core field. The rate of dipole decrease is variable, but on average it is about one order of magnitude faster than predicted by free decay (Olson & Amit 2006), so it is likely that the trends shown in Fig. 1 are a consequence of both advective (Roberts & Scott 1965) and diffusive (Gubbins 1987) processes operating simultaneously. Importantly however, the effects of advection and diffusion may not operate equally over the whole spherical harmonic spectrum of the core field. Because the magnetic Reynolds number of the core is large (e.g. Bloxham & Jackson 1991), it is expected that advection effects play a proportionally larger role in the geomagnetic secular variation (SV) on the largest scales (i.e. for the lowest spherical harmonics), whereas diffusion plays a proportionally larger role on the smaller scales (i.e. for higher spherical harmonics).

In this paper, we propose a simple cascade model that connects the dipole moment decrease to the time evolution of the energy spectrum of the core field. The model assumes that magnetic energy SV is dominated by transfer between adjacent spherical harmonic degrees by fluid motions in the outer core. Our model is motivated by the trends evident in Fig. 1 and supported by results of numerical dynamo simulations, which show qualitatively similar spectral transfer effects during times of rapid dipole collapse, events that sometimes precede polarity reversals and excursions. We apply our cascade model to estimate the rates of spectral transfer in the core during the present-day dipole decrease.

2 GEODYNAMO CASCADE MODEL

The average magnetic energy density of the core field on the CMB is proportional to R, the mean squared field intensity at the core radius $r = c$. The spectrum of R, called the Mauersberger–Lowes

spectrum, is conventionally written as

$$R = \sum_{n=1}^{n_{\max}} R_n, \tag{1}$$

where n is spherical harmonic degree and $n_{\max}$ is the truncation, usually $n_{\max} \simeq 14$ for the core field. The Mauersberger–Lowes spectrum at the CMB is one of the primary constraints on the dynamo process in the core (Dormy *et al.* 2000). The terms R_n at the CMB can be expressed as sums of squares of the Gauss coefficients of the core field, according to (Lowes 1974)

$$R_n = (n+1)\left(\frac{a}{c}\right)^{2n+4} \sum_{m=0}^{n} \left(\left(g_n^m\right)^2 + \left(h_n^m\right)^2 \right), \tag{2}$$

where a is Earth's radius and g_n^m and h_n^m are the Gauss coefficients of the core field in mT at spherical harmonic degree and order n and m, respectively. The mean squared field intensity can also be defined for the equatorially antisymmetric part of the core field termed the dipole family by summing (2) over odd values of $n-m$, and for the equatorially symmetric part of the core field termed the quadrupole family by summing over even values of $n-m$ (Roberts 1971). In this paper, we denote spectra with these symmetries using superscripts a and s, for example R_n^a and R_n^s, respectively.

Using (2), the time variation of the spectrum of R is written as (Cain *et al.* 1989)

$$\dot{R}_n = 2\,(n+1)\left(\frac{a}{c}\right)^{2n+4} \sum_{m=0}^{n} \left(g_n^m \dot{g}_n^m + h_n^m \dot{h}_n^m \right), \tag{3}$$

where the dot denotes time derivative. Like the Mauersberger–Lowes spectrum, (3) can be split into its equatorially antisymmetric and symmetric parts, denoted here by $\dot{R}_n^a$ and $\dot{R}_n^s$, respectively. Note that (3) which has units of $\mathrm{mT^2 yr^{-1}}$ differs from the definition of the spectrum of the SV field itself at the CMB, which has units of $\mathrm{mT^2 yr^{-2}}$ and is given by (Alldredge 1984; McLeod 1996; Voorhies 2004)

$$S_n = (n+1)\left(\frac{a}{c}\right)^{2n+4} \sum_{m=0}^{n} \left(\left(\dot{g}_n^m\right)^2 + \left(\dot{h}_n^m\right)^2 \right). \tag{4}$$

Temporal changes in the shape of the Mauersberger–Lowes spectrum are reflected in non-uniform time variations in the individual terms $\dot{R}_n$, $\dot{R}_n^a$, $\dot{R}_n^s$, S_n, S_n^a or S_n^s.

A cascade model for the evolution of R_n can be derived starting from the radial component of the magnetic induction equation at the top of the core. Assuming incompressible flow, the radial component of the induction equation at the CMB is

$$\frac{\partial B_r}{\partial t} + \mathbf{u}_h \cdot \nabla B_r + B_r \nabla_h \cdot \mathbf{u}_h = \eta \hat{r} \cdot \nabla^2 \mathbf{B}, \tag{5}$$

where B_r is the radial component of the magnetic field on the CMB, t is time, $\mathbf{u}_h$ is the free stream fluid velocity in the outer core below the CMB, r is the radial coordinate, $\hat{r}$ is its unit vector, η is the magnetic diffusivity of the outer core, $\mathbf{B}$ the magnetic field vector on the CMB and the subscript h denotes coordinates tangent to the CMB. The first term on the left-hand side of (5) is the SV, the second and third terms on the left-hand side represent advection of magnetic field by the flow, and the term on the right-hand side represents magnetic diffusion. Units of all these variables are given in Table 1.

Multiplying (5) by B_r and averaging over the CMB gives

$$\frac{\partial}{\partial t}\left\langle B_r^2 \right\rangle = -\left\langle \mathbf{u}_h \cdot \nabla B_r^2 \right\rangle - 2\left\langle B_r^2 \nabla_h \cdot \mathbf{u}_h \right\rangle + 2\eta \left\langle B_r \hat{r} \cdot \nabla^2 \mathbf{B} \right\rangle, \tag{6}$$

where $\langle\ \rangle$ denotes CMB surface average. The left hand side of (6) is the time derivative of the mean square radial field. Using the relationship

$$\left\langle B_r^2 \right\rangle = \sum_{n=1}^{n_{\max}} \frac{n+1}{2n+1} R_n, \tag{7}$$

(6) can be written symbolically for each spherical harmonic degree as

$$\dot{R}_n = T_n - D_n \tag{8}$$

where

$$T_n = -\frac{2n+1}{n+1}\left(\left\langle \mathbf{u}_h \cdot \nabla B_r^2 \right\rangle_n + 2\left\langle B_r^2 \nabla_h \cdot \mathbf{u}_h \right\rangle_n \right) \tag{9}$$

is the transfer spectrum of the core field and

$$D_n = -2\frac{2n+1}{n+1}\eta \left\langle B_r \hat{r} \cdot \nabla^2 \mathbf{B} \right\rangle_n \tag{10}$$

is its diffusion spectrum, both at harmonic degree n. In the following subsections we develop parametrized representations for both the diffusion spectrum D_n and the transfer spectrum T_n.

2.1 Diffusion spectrum

The exact form of magnetic diffusion in the core cannot be deduced from the geomagnetic field at the CMB, and therefore the diffusion terms in (5) and (6) cannot be inferred from observations. However, we can estimate a lower limit on the diffusion spectrum D_n from the rate of free decay of the core field at each harmonic degree n, as follows. The radial field on the CMB is given in terms of the Gauss coefficients by

$$B_r = \sum_{n=1}^{n_{\max}} \sum_{m=0}^{n} {B_r}_n^m = \sum_{n=1}^{n_{\max}} \sum_{m=0}^{n} \left(\frac{a}{c}\right)^{n+2} (n+1)\, P_n^m(\cos\theta) \times \left(g_n^m \cos m\phi + h_n^m \sin m\phi \right), \tag{11}$$

where ${B_r}_n^m$ is the radial field contribution of degree n and order m, P_n^m are the Legendre functions, θ is colatitude and ϕ is longitude. Focusing on free decay, the diffusion term in (5) can be rewritten using (11) as

$$\eta \hat{\mathbf{r}} \cdot \nabla^2 \mathbf{B} = -\frac{\eta}{c^2} \sum_{n=1}^{n_{\max}} \sum_{m=0}^{n} {p_n^j}^2 {B_r}_n^m, \tag{12}$$

where p_n^j denote the free decay eigenvalues of each mode j. The eigenvalues p_n^j correspond to the roots of the Bessel function $J_{(n-1/2)}(p_n^j) = 0$ (see Moffatt 1978), the smallest root at a given n corresponding to the fundamental mode p_n, and the larger roots corresponding to the higher modes, which have more radial structure in the core and therefore diffuse faster. Multiplying both sides of (12) by (11), summing over m, and averaging the resulting expression at the CMB, we obtain the following representation of the diffusion spectrum at harmonic degree n:

$$D_n = 2\frac{\eta}{c^2} p_n^2 R_n, \tag{13}$$

where we choose for simplicity the fundamental mode p_n. Although (13) is not a complete model for magnetic diffusion, it serves to define the fundamental timescales for free decay at each spherical harmonic

$$\tau_n^d = \frac{c^2}{2\eta p_n^2}. \tag{14}$$

Table 1. Summary of variables and their dimensions. MKS units are: T is Tesla, m is metres, s is seconds, and Γ is a any tracer such as temperature or chemical concentration. In the text we sometimes use other units, e.g. mT, km, yr. Note that all variables are also defined for the equatorially asymmetric dipole family and the equatorially symmetric quadrupole family by the superscripts *a* and *s*, respectively.

Variable	Symbol	Dimension
Spherical radial, colatitude and longitude coordinates	r, θ and ϕ	m and radians
Cartesian wavenumber	k	m^{-1}
Spherical harmonic degree and order	n and m	–
Legendre function	P_n^m	–
Earth's surface radius	a	m
Earth's core radius	c	m
Gauss coefficients	g_n^m and h_n^m	T
Magnetic energy spectrum	R_n	T^2
SV of Magnetic energy spectrum	$\dot{R}_n$	$\mathrm{T}^2\ \mathrm{s}^{-1}$
SV spectrum	S_n	$\mathrm{T}^2\ \mathrm{s}^{-2}$
Radial magnetic field	B_r	T
Radial magnetic field of harmonic n and m	$B_{r\,n}^{\ m}$	T
Rms magnetic field	B_{rms}	T
Magnetic field vector	$\mathbf{B}$	T
Time	t	s
Tangential velocity vector	$\mathbf{u}_h$	$\mathrm{m\ s}^{-1}$
Magnetic diffusivity	η	$\mathrm{m}^2\ \mathrm{s}^{-1}$
Free decay eigenvalues	p_n^j	–
Fundamental free decay mode	p_n	–
Fundamental free decay timescale	τ_n^d	s
Cartesian scalar variable	Γ_k	Γ
Cartesian scalar energy spectrum	R_k	Γ
SV of Cartesian scalar variable	$\dot{\Gamma}_k$	$\Gamma\ \mathrm{s}^{-1}$
Cartesian transfer spectrum	T_k	$\Gamma\ \mathrm{s}^{-1}$
Diffusivity of Cartesian scalar variable	κ	$\mathrm{m}^2\ \mathrm{s}^{-1}$
Cartesian flux spectrum	F_k	$\Gamma\ \mathrm{ms}^{-1}$
Cartesian spectral transfer rate	γ_k	$\mathrm{m\ s}^{-1}$
Spherical transfer spectrum	T_n	$\mathrm{T}^2\ \mathrm{s}^{-1}$
Spherical diffusion spectrum	D_n	$\mathrm{T}^2\ \mathrm{s}^{-1}$
Spherical flux spectrum	F_n	$\mathrm{T}^2\ \mathrm{s}^{-1}$
Spherical spectral transfer rate	γ_n	s^{-1}
SV timescale based on S_n	τ_n	s
SV timescale based on $\dot{R}_n$	τ_n^*	s

Slow spectral variations correspond to $\dot{R}_n$-values small compared to fundamental mode D_n-values, and conversely, rapid spectral variations correspond to $\dot{R}_n$-values large compared to the same D_n-values. Our cascade model is intended for the fast spectral change regime.

2.2 Transfer spectrum

We model the transfer spectrum T_n of the core field as a cascade process, on the basis of the similarity between (8) and the equation governing spectral evolution of a scalar variable in a turbulent flow. In the classical Kolmogorov description of hydrodynamic turbulence, energy is exchanged between similar size eddies without major jumps from one scale to another (Frisch 1995). This Kolmogorov type of energy transfer is usually referred to as *local*, and the term *cascade* is often used to describe the transfer process. In this paper, we use the term *local* for the transfer of magnetic energy between adjacent harmonics in spectral space. A *forward* cascade denotes energy transfer from large to small scales, or in our case, from lower to higher spherical harmonics. Conversely, an *inverse* cascade denotes energy transfer from higher to lower harmonics.

Analyses of numerical simulations of magnetohydrodynamic (MHD) turbulence (Alexakis *et al.* 2007) associate these two types of spectral transfer with different terms in the induction equation. Local magnetic energy transfer is associated with advection of magnetic field by the flow (first term on the right-hand side of 9), whereas non-local transfer is associated with magnetic field stretching (second term on the right-hand side of 9). For non-rotating MHD turbulence, Alexakis *et al.* (2007) find that the non-local transfer of magnetic energy due to stretching actually dominates over local magnetic energy transfer by direct energy advection. In addition, recent core flow models argue that non-local transfer, in the form of interactions between small-scale field and large-scale flow or small-scale flow and large-scale field leading to small-scale SV, dominates their model misfit (Eymin & Hulot 2005; Pais & Jault 2008). However, we argue that local spectral transfer is the dominant process that shapes the core field spectrum, because so much of the core field SV can be explained as frozen-flux advection by an evolving large-scale dominantly toroidal flow (e.g. Jackson 1997; Amit & Olson 2006) with the non-local energy transfer from smaller scales being of secondary importance.

In terms of Cartesian wavenumbers k, the spectral evolution equation of a scalar variable subject to advection and diffusion is

commonly written as (Hill 1978)

$$\dot{\Gamma}_k = T_k - 2\kappa k^2 \Gamma_k, \tag{15}$$

where Γ_k is the wavenumber spectrum of the scalar variable, T_k is the transfer spectrum, and κ is the diffusivity of the scalar variable. Local cascade models relate T_k to a quantity called the flux spectrum F_k via

$$T_k = -\frac{\partial}{\partial k} F_k. \tag{16}$$

Physically, this spectrum F_k represents the flux of magnetic energy through wavenumber space. It is often assumed that the flux spectrum F_k is linked to the energy spectrum R_k via

$$F_k = \gamma_k R_k, \tag{17}$$

where γ_k is the spectral transfer rate in units of velocity (Corrsin 1961, 1964). In general, all quantities in (17) are functions of both wavenumber and time. However, under conditions of statistical equilibrium, the time dependence of γ_k in (17) is assumed to vanish, and in this situation it is often found that γ_k can be approximated as a power-law function of k. For example, a standard form of γ_k for the spectrum of a passive scalar in homogeneous isotropic turbulence is (Hill 1978; Frisch 1995)

$$\gamma_k \propto k^{5/3}. \tag{18}$$

At the top of Earth's core the flow is neither isotropic nor homogeneous (due to the rotational effect and mantle control), so although the 5/3 Kolmogorov exponent may not hold, it has been proposed that a general power law of the form (18) is applicable there (Voorhies 2004).

The preceding discussion applies to continuous wavenumber spectra. For spherical harmonic spectra, there is a close analogy between (8) and (15) in the asymptotic limit of large n, for which $kc = \sqrt{n\,(n+1)}$ becomes a good approximation (Backus *et al.* 1996). However, the correspondence is not exact because k is continuous while n is discrete (see Appendix B4 of Voorhies 2004). Accordingly, in place of (16), we hypothesize that the spectral transfer and spectral flux are related by the following difference formula

$$T_n = F_{n-1} - F_n. \tag{19}$$

Note that the dependence of T on F in (19) involves only nearest-neighbour spectral terms, consistent with our local spectral transfer assumption. Substituting (19) into (8) then yields the following recursion formula for the flux spectrum:

$$F_n = F_{n-1} - \dot{R}_n - D_n \tag{20}$$

with the initial value $F_0 = 0$ (corresponding to zero geomagnetic monopole). We further hypothesize that, by analogy with (17) the flux spectrum F_n and Mauersberger–Lowes spectrum R_n are related by

$$F_n = \gamma_n R_n, \tag{21}$$

where γ_n represents the local rate of transfer through the Mauersberger–Lowes spectrum in units of reciprocal time (Table 1). According to (21), γ_n is just given by F_n/R_n. However, to avoid singularities where R_n is small, we obtain smoother and more stable results if we calculate γ_n as

$$\gamma_n = \frac{F_n + F_{n+1}}{R_n + R_{n+1}} \tag{22}$$

in which case γ_n in our model represents the rate of transfer from spherical harmonic degree n to degree $n+1$. With this definition, positive values of γ_n correspond to a forward cascade of magnetic energy through the Mauersberger–Lowes spectrum (from n to $n+1$), whereas negative values of γ_n correspond to an inverse magnetic energy cascade (from $n+1$ to n).

Although our model assumes only local spectral transfer, it is important to point out that non-local spectral transfer may be important in the geodynamo, particularly as it contributes to the dipole moment. Non-local spectral transfer is sometimes observed in non-magnetic turbulence, both in experiments (Wiltse & Glezer 1993) and in numerical simulations (Alexakis *et al.* 2005). Spectral transfer is well established in MHD turbulence (Maron & Goldreich 2001; Biskamp 2003; Müller & Grappin 2005; Boldyrev 2006). Numerical simulations show that the spectral transfer typically consists of two components, one local and Kolmogorov-like, the other non-local, in which the magnetic energy jumps discontinuously from small-scales to large-scales (Yousef *et al.* 2007). Theoretically, this type of non-local transfer is implicit in the α-dynamo effect (Moffatt 1978; Biskamp 2003). It is also linked to magnetic helicity, which is thought to be a vital ingredient in the generation of large-scale magnetic fields from small-scale turbulent flows in astrophysical bodies (Pouquet *et al.* 1976; Cho *et al.* 2002).

2.3 Analytical tests of local spectral transfer

The relationship between the transfer spectrum and the flux spectrum (16) holds if the spectral transfer is local, but may give spurious results in situations where the spectral transfer is non-local. In addition, our finite difference (19) and smoothing (22) approximations might constitute additional sources of error in some situations. Here we use analytical examples in which we specify the spectral transfer, in order to show where our model assumptions work and where they breakdown.

The first examples are of purely local spectral transfer, so these serve to test our method of calculating γ_n. We specify the actual local spectral transfer rate $\tilde{\gamma}_n$ as the net magnetic energy transfer from degree n to degree $n+1$ in the Mauersberger–Lowes spectrum, normalized by R_n, and located in spectral space at n. For simplicity in this section we adopt the frozen-flux limit, so the diffusion term D_n is ignored. Accordingly, the relationship between the actual local spectral transfer rate $\tilde{\gamma}_n$, the Mauersberger–Lowes spectrum R_n and its SV $\dot{R}_n$ is

$$\dot{R}_n = \tilde{\gamma}_{n-1} R_{n-1} - \tilde{\gamma}_n R_n. \tag{23}$$

Also note that in the frozen-flux limit our model F_n (20) yields

$$F_n = -\sum_{q=1}^{n} \dot{R}_q. \tag{24}$$

Consider a decreasing dipole field with $\dot{R}_1 < 0$ in which the dipole energy is transferred to successively higher harmonics at a uniform rate, while the non-dipole part of the Mauersberger–Lowes spectrum is constant in time. The situation is sketched in Fig. 2(a). Further assume in this first example that the Mauersberger–Lowes spectrum is flat, that is, $R_n = R_1$. Then according to (23), $\tilde{\gamma}_n = -\dot{R}_1/R_1$ is the actual spectral transfer rate through the Mauersberger–Lowes spectrum. For comparison, our model gives $F_n = -\dot{R}_1$ according to (24), and according to (22) $\gamma_n = -\dot{R}_1/R_1$, identical to the actual transfer rate.

If the field spectrum is not flat, then the spectral transfer rates in our model will not be identical to the actual ones. However, the two will be very close if the Mauersberger–Lowes spectrum has a continuous variation with n. Consider for instance the same transfer

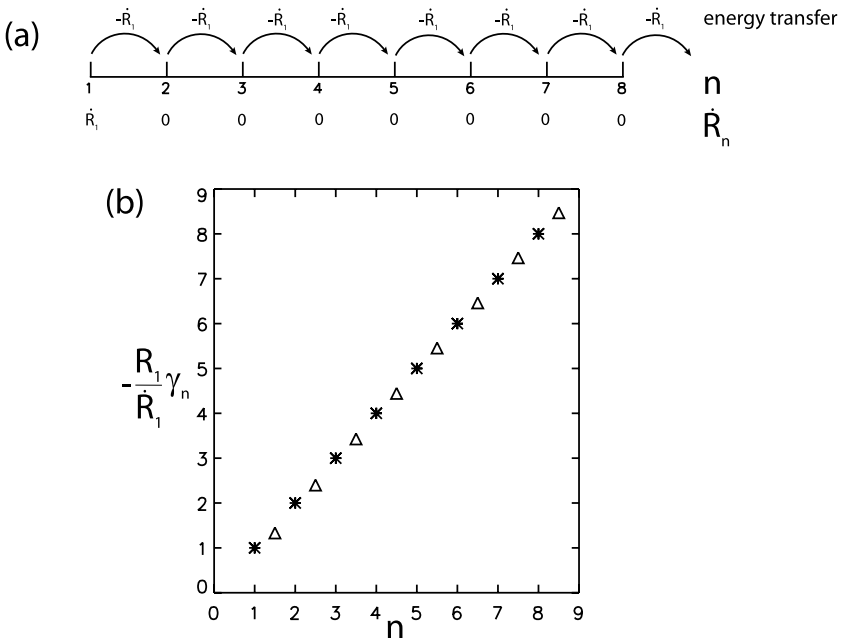

Figure 2. (a) Schematic illustration of a uniform, local, forward energy cascade. (b) Normalized spectral transfer rates versus spherical harmonic degree n with $R_n = R_1/n$: actual values $-(R_1/\dot{R}_1)\tilde{\gamma}_n$ (25) denoted by asterisks versus the model $-(R_1/\dot{R}_1)\gamma_n$ (26) denoted by triangles. The positions of the model γ_n have been shifted by one half unit of n to represent transfer between harmonics n and $n+1$.

from the dipole field as in the previous example, but in this case assume $R_n = R_1/n$ for the Mauersberger–Lowes spectrum. Then according to (23)

$$\tilde{\gamma}_n = -n\frac{\dot{R}_1}{R_1}, \tag{25}$$

whereas according to (22) and (24)

$$\gamma_n = -n\frac{\dot{R}_1}{R_1}\frac{2n+2}{2n+1}. \tag{26}$$

As shown in Fig. 2(b), the difference between our model rates (26) and the actual rates (25) are minor, particularly with increasing n.

A second example again assumes local spectral transfer but allows for time variation in the non-dipole as well as the dipole parts of the Mauersberger–Lowes spectrum. Consider as before a decreasing dipole field with $\dot{R}_1 < 0$, but in this case the forward cascade is non-uniform, and transfers successively smaller amounts of magnetic energy towards successively higher degrees n (Fig. 3a). This results in an increasing non-dipole spectrum in which

$$\dot{R}_{n>1} = -\alpha\dot{R}_1, \tag{27}$$

where α is the fractional difference in the energy transferred from one harmonic to the next higher. Although this is just a slight extension of the first examples, it is an idealization of the historical behaviour of the core field. Assuming as in the previous case that $R_n = R_1/n$, (23) and (27) give for the actual transfer rate

$$\tilde{\gamma}_n = -n\frac{\dot{R}_1}{R_1}\left(1-(n-1)\,\alpha\right), \tag{28}$$

whereas according to (22), (24) and (27), the model values are

$$\gamma_n = -n\frac{\dot{R}_1}{R_1}\frac{n+1}{2n+1}\left(2-(2n-1)\,\alpha\right). \tag{29}$$

Figs 3(b)–(e) compare between (28) and (29) for several values of the parameter α. As in the previous examples, the agreement is excellent. According to (28) and (29), the cascade is forward ($\gamma > 0$) up to $n = N$, where

$$N = \frac{\alpha+\epsilon}{\epsilon\alpha}, \tag{30}$$

where $\epsilon = 1$ for the actual transfer and $\epsilon = 2$ for our model. For $n > N$, the γ-coefficients change sign. In these situations, our model interpretation is that magnetic energy cascading up the spectrum becomes absorbed (trapped) in the spectral band $2 \le n \le N$.

For the geodynamo, spectral transfer of magnetic energy is more complex than these simple examples, involving a combination of local, non-local, forward and inverse cascades (Fig. 4a). To illustrate how our local spectral transfer model treats non-local spectral transfer, consider the situation shown in Figs 4(b) and (c). In these cases, energy from the dipole is transferred directly to some higher harmonic n' beyond (Fig. 4b) or within (Fig. 4c) the observable core field spectrum, while all other harmonics experience zero net transfer. In this case our model incorrectly predicts a continuous forward cascade from $n = 1$ to $n = n' - 1$ (as in e.g. (26) and Fig. 2), while the actual spectral transfer is non-local, that is, $\tilde{\gamma}_n = 0$. Although this example demonstrates the pitfalls in distinguishing between local and non-local transfer effects, it also suggests there are warning signs, such as abrupt changes in the inferred spectral transfer rate, which indicate where the transfer is non-local.

Even though it is not possible to uniquely distinguish local from non-local spectral transfer, there are some situations that strongly favour the local transfer interpretation. For example, consider the case in which a local peak in the Mauersberger–Lowes spectrum is observed to propagate towards higher degrees over time. As illustrated in Figs 5(a) and (b), the energy peak centred at n' at time t_0 propagates to degree $n'+1$ at time $t_0 + \delta t$. The amplitude of the peak is δR relative to the background level R_1 of the spectrum. In this case, the actual spectral transfer rates in the neighbourhood of

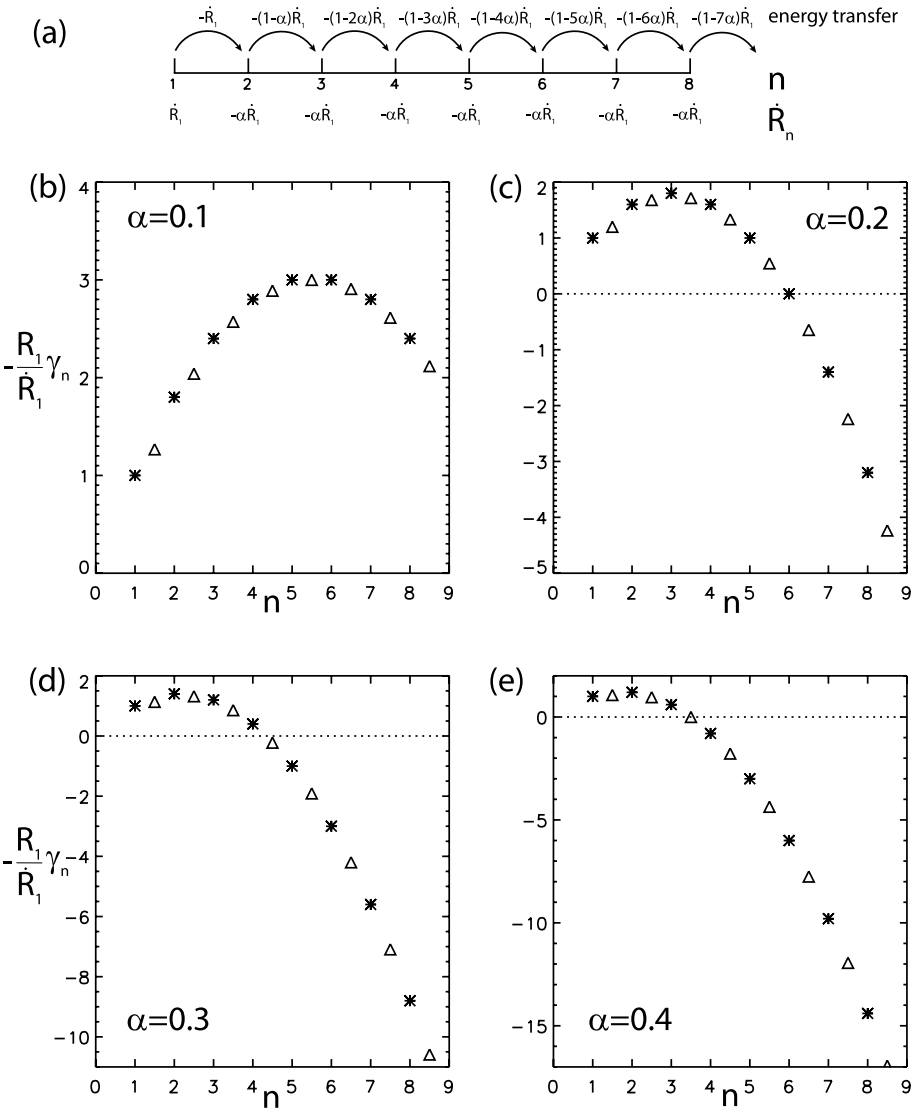

Figure 3. As in Fig. 2 for a non-uniform, local, forward energy cascade (28)–(29). In (b)–(e) the spectral transfer rates are given for various α values.

the peak are

$$\tilde{\gamma}_{n'-1} = \tilde{\gamma}_{n'+1} = \frac{1}{\delta t}\frac{\delta R}{2R_1 + \delta R}$$
$$\tilde{\gamma}_{n'} = \frac{1}{\delta t}\frac{\delta R}{R_1 + \delta R}, \tag{31}$$

whereas our model rates in the same neighbourhood are

$$\gamma_{n'-2} = \gamma_{n'+1} = \frac{1}{\delta t}\frac{\delta R}{4R_1 + \delta R}$$
$$\gamma_{n'-1} = \gamma_{n'} = \frac{1}{\delta t}\frac{3\delta R}{4R_1 + 3\delta R}. \tag{32}$$

Again our model captures well the actual rates, independently of the peak-to-background ratio (Figs 5c and d).

In Fig. 6(c) a travelling peak that propagates from higher towards lower degrees in the quadrupole family of the Mauersberger–Lowes spectrum is evident in the geomagnetic core field. For this structure, the peak-to-background amplitude is $(R_1 + \delta R)/R_1 \sim 4$, comparable to the propagating example used in Fig. 5(d). Because our model is shown to recover the propagation direction, location in spectral space and speed, we suggest that the evolution of this particular structure in Fig. 6(c) is evidence for local energy transfer in the geomagnetic field.

2.4 Spectral transfer rates and secular variation timescales

The traditional measures of core field variations are the SV timescales τ_n, which in our notation are defined as

$$\tau_n = \sqrt{\frac{R_n}{S_n}} \tag{33}$$

(Hulot & LeMouël 1994; McLeod 1996; Hongre *et al.* 1998; Christensen & Tilgner 2004; Holme & Olsen 2006; Gillet *et al.* 2009). The magnitude of τ_n may vary significantly from one epoch to another (Hulot & LeMouël 1994). Voorhies (2004) argued that the timescale

$$\tau_n^* = \frac{R_n}{|\dot{R}_n|} \tag{34}$$

based on the SV of the spectrum $\dot{R}_n$ is more relevant than τ_n which is based on the spectrum of SV S_n. Physical interpretation of (33)

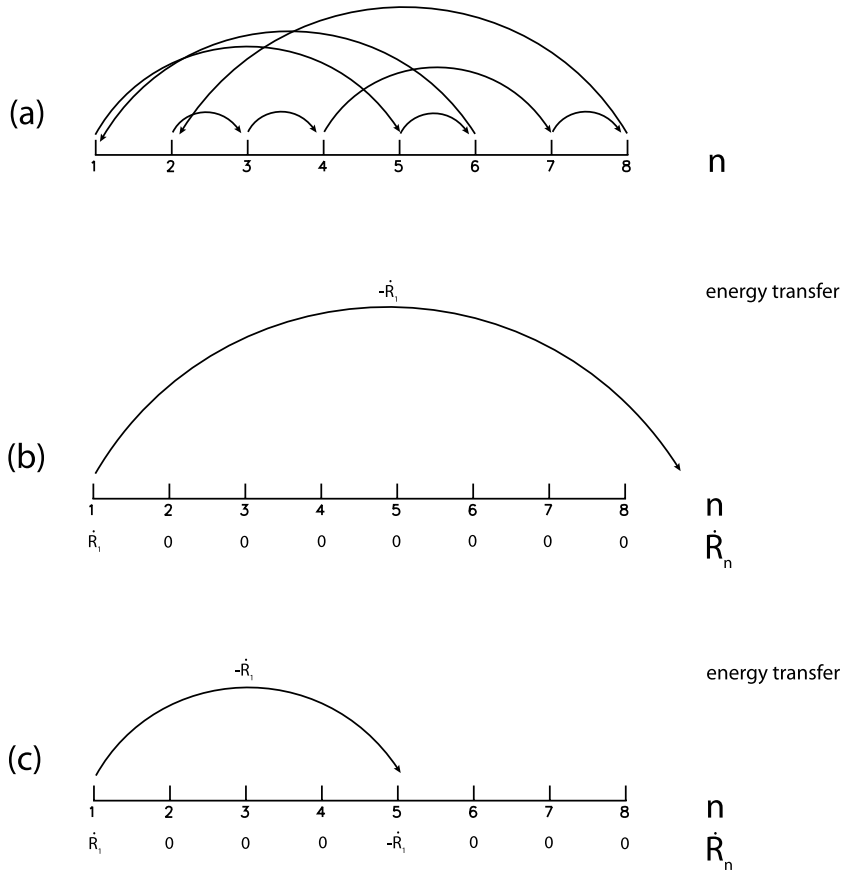

Figure 4. Schematic illustrations of non-local transfer. (a) A general mixed state of local, non-local, forward and inverse cascades. (b) Non-local transfer from the dipole to a degree higher than the observable spectrum. (c) Non-local transfer from the dipole to a high degree within the observable spectrum.

and (34) depends strongly, although implicitly, on the dominant processes that control the SV at each spherical harmonic degree. At low magnetic Reynolds number conditions for example, (33) represents free decay timescales for each harmonic of the field, whereas at high magnetic Reynolds number conditions, (33) represents a combination of spectral transfer by advection and diffusion (Liu & Olson 2009). Hulot & LeMouël (1994) determined τ_n for the non-axial dipole field to be on the order of several centuries, with decreasing values for higher degrees. The axial dipole timescale is longer than the timescales of other harmonics (Lowes 1974; Alldredge 1984). Hulot & LeMouël (1994) argued that diffusive effects dominate the axial dipole behaviour, whereas advection dominates the other timescales. They also showed that, apart from the axial dipole term, the dipole and quadrupole families have similar τ_n-values. Christensen & Tilgner (2004) found they could match core field SV timescales for $n > 2$ with the τ_n-values from a numerical dynamo model with a large magnetic Reynolds number, $Rm \simeq 500$. Spectral transfer processes certainly play an important role in this regime of Rm. Another piece of supporting evidence are the very short timescales at the harmonics on the edge of the core field at $n \simeq 14$. Assuming power law fit for τ_n in the range $n = 3 - 12$, satellite geomagnetic field models predict $\tau_{14} \simeq 20$ yr for the highest degrees in the core field (Holme & Olsen 2006; Gillet *et al.* 2009). Another short timescale relevant to the geomagnetic field is the dynamo memory, the time required for the perturbed and unperturbed dynamos to diverge. Hulot *et al.* (2010) inferred this is about one century for the geodynamo.

Our spectral transfer rates γ_n conceptually differ from both the SV timescales τ_n and from τ_n^* in several respects. Most importantly, γ_n can be positive or negative, its sign indicating the energy cascade direction. A more subtle difference is that $1/\tau_n$ and $1/\tau_n^*$ are related to the rate of field change at a particular harmonic degree, whereas γ_n refers to the rate at which energy transfers by one harmonic degree. In spite of these differences, we show in the next section that there are similarities between $1/\tau_n$ and the magnitude of γ_n in the historical field behaviour.

3 SPECTRAL CASCADE AND GEOMAGNETIC DIPOLE DECREASE

We use the historical field model *gufm1* on the CMB for the period 1840–1990 (Jackson *et al.* 2000) and the field model *xCHAOS* on the CMB for the period 1999–2009 (Olsen & Mandea 2008) to interpret the geomagnetic dipole decrease shown in Fig. 1 in terms of a spectral cascade. For each core field model, we first calculate R_n and its time derivative $\dot{R}_n$ on the CMB. To avoid artefacts due to temporal variations in the resolution of *gufm1*, we truncate this field model at degree and order $n_{\max} = m_{\max} = 8$, whereas we truncate the *xCHAOS* field model at $n_{\max} = m_{\max} = 14$. Fig. 6(a) shows the Mauersberger–Lowes spectrum of the historical geomagnetic field on the CMB as a function of time, and Figs 6(b) and (c) show the corresponding Mauersberger–Lowes spectra for the dipole and quadrupole families, respectively. The same spectra for the

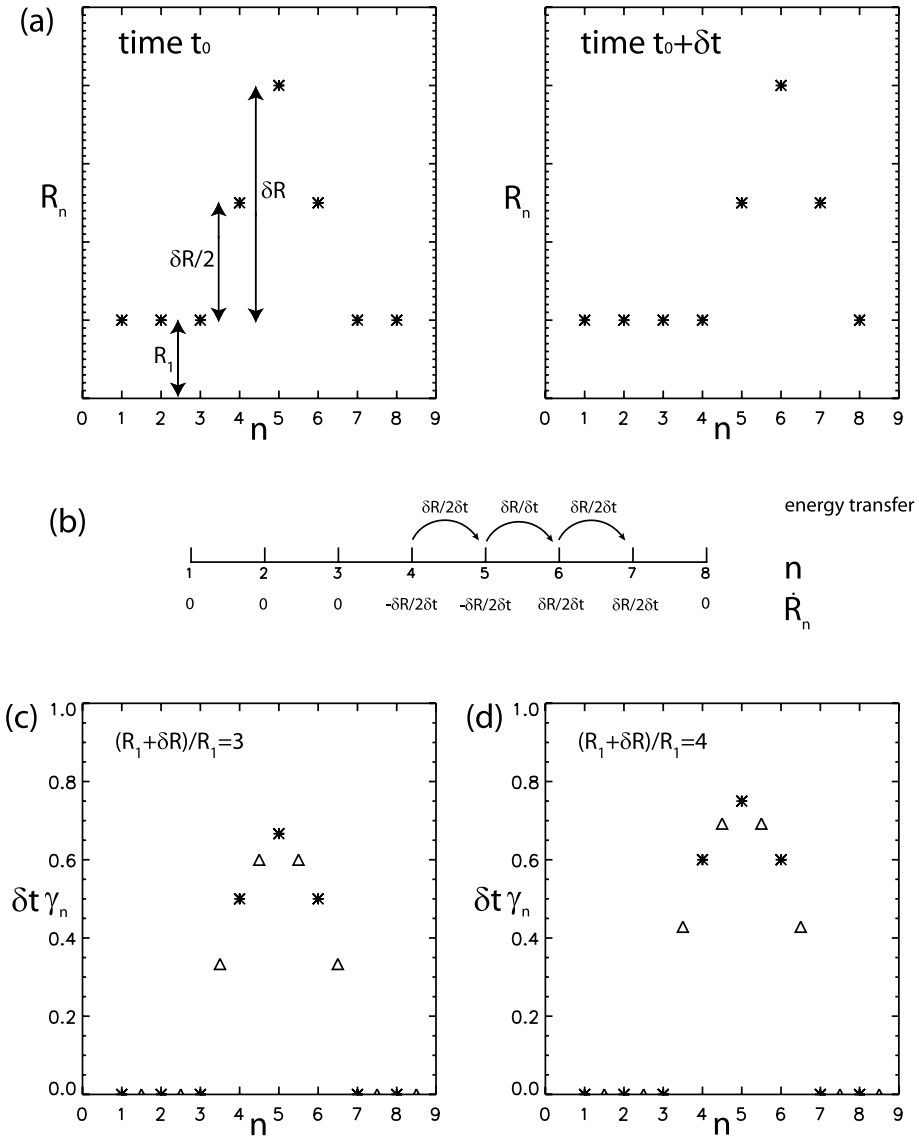

Figure 5. (a) The Mauersberger–Lowes spectra of a peak travelling between times t_0 to $t_0 + \delta t$ from n' to $n' + 1$, and (b) a schematic illustration of the energy cascade. The background flat spectrum is R_1 and the peak is elevated by δR. Normalized spectral transfer rates versus spherical harmonic degree n for a peak-to-background ratios of $(R_1 + \delta R)/R_1 = 3$ (c) and $(R_1 + \delta R)/R_1 = 4$ (d): actual values $\delta t \tilde{\gamma}_n$ (31) denoted by asterisks versus the model $\delta t \gamma_n$ (32) denoted by triangles. The positions of the model γ_n have been shifted by one half unit of n to represent transfer between harmonics n and $n + 1$.

1999–2009 core field are shown in Figs 6(d)–(f). These contour plots provide some qualitative evidence for geomagnetic energy cascade, in the form of migration of local maxima and minima from one n-value to its neighbours over time, for example, in the dipole family spectrum from $n = 3$ to 4 and from $n = 5$ to 6 (Fig. 6b), and more pronouncedly in the quadrupole family spectrum from $n = 5$ through 4 to 3 (Fig. 6c).

The next step is to calculate the flux spectra F_n from (20) using $\dot{R}_n$ from Fig. 6 and diffusion spectra D_n from (13), in which we use the fundamental mode eigenvalues for p_n and assume $\eta = 2\,\mathrm{m^2\,s^{-1}}$ for the magnetic diffusivity of the outer core (well within the range of estimated values, see Poirier 2000). Table 2 lists the first 14 fundamental free decay modes and the corresponding free decay timescales. Fig. 7 shows the time dependence of F_n obtained this way. The black curves are derived from $\dot{R}_n$ and D_n at $n = 1$, whereas the coloured F_n curves are derived from the $\dot{R}_n$ and D_n degrees from 1 to n. In general, we find that D_n increases with n, but in nearly all cases $|D_n| \ll |\dot{R}_n|$, that is, the impact of fundamental mode diffusion on the flux spectrum of the core field is of secondary importance.

To illustrate how the recursion formula (20) works, consider Fig. 7(a). The black curve is the most positive because the dipole decreases, while the other curves are in general successively smaller due to the pervasive increase of most non-dipole components, in agreement with uniform flux convergence in the non-dipole part of the spectrum and consistent with local transfer. Crossing of individual F_n curves is produced by instantaneous decrease of some non-dipole harmonics, and this may indicate deviations from purely local transfer.

The final step is to compute the spectral transfer rates γ_n from F_n and R_n using (22). In Fig. 8, we compare the time average of the absolute spectral transfer rates $|\gamma_n|$ with the time average $1/\tau_n$ defined in (33). The positions of the spectral transfer rates have been shifted by one half unit of n in Fig. 8 (and in subsequent figures) in order to emphasize that they represent transfer between a pair of

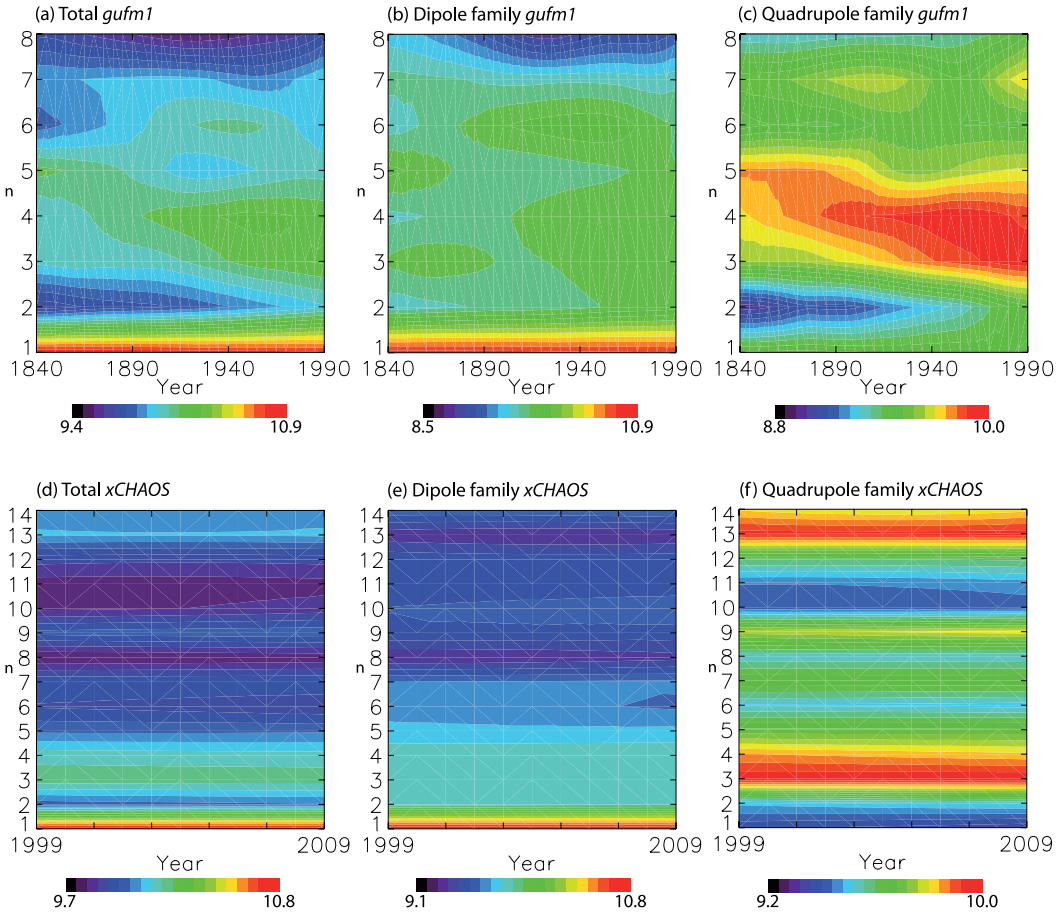

Figure 6. The Mauersberger–Lowes spectra of the geomagnetic field at the core–mantle boundary as a function of time. Spectral values are defined only at integer spherical harmonic degrees n. For the period 1840–1990 from core field model *gufm1* (Jackson *et al.* 2000) with $n_{\max} = 8$: (a) full field; (b) dipole family; (c) quadrupole family. For the period 1999–2009 from core field model *xCHAOS* (Olsen & Mandea 2008) with $n_{\max} = 14$: (d) full field; (e) dipole family; (f) quadrupole family. The log-scale ranges of the spectra in nT^2 are given in the colour bars.

Table 2. Fundamental free decay modes p_n, and free decay timescales τ_n^d in years based on magnetic diffusivity of $\eta = 2\ \mathrm{m^2 s^{-1}}$, for spherical harmonic degrees $n = 1 - 14$.

Degree	p_n	τ_n^d [yr]
1	π	9733
2	4.493	4758
3	5.763	2892
4	6.988	1967
5	8.183	1435
6	9.356	1097
7	10.513	869
8	11.657	707
9	12.790	587
10	13.916	496
11	15.033	425
12	16.145	369
13	17.250	323
14	18.351	285

neighbouring harmonics. The overall magnitudes of the two rates are comparable at low degrees in the total field and in both the dipole and quadrupole families. Also, their trends are similar up to spherical harmonic degree $n = 8$ in the total field, $n = 7$ in the dipole family, and $n = 6$ in the quadrupole family, although there are substantial differences at higher degrees. The absolute spectral transfer rates in Fig. 8 tend to be less than the corresponding SV rates $1/\tau_n$ for the total field because γ_n can have either sign, whereas τ_n is not. The dipole family γ_n^a are dominantly positive, whereas the quadrupole family γ_n^s are dominantly negative, so the absolute rates for the total field are smaller than those for each family. The generally monotonic variations of γ_n with n in Fig. 8 is suggestive of the power-law spectral transfer rates commonly found in turbulence measurements (Corrsin 1961, 1964; Hill 1978). This behaviour is consistent with (although does not prove) our interpretation of local, nearest-neighbour energy transfer through the geomagnetic spectrum.

4 DIPOLE COLLAPSE AND SPECTRAL TRANSFER IN A NUMERICAL DYNAMO

Numerical dynamos show energy cascade behaviour, especially during dipole collapse events that precede polarity reversals or excursions (Olson *et al.* 2009). Although these events involve both magnetic advection and diffusion, even at very high magnetic Reynolds numbers (Liu & Olson 2009), there are time intervals when the net effects of diffusion on the low harmonic degree part of the magnetic field are negligibly small. During these time intervals, the mean square field intensity on the outer boundary of the

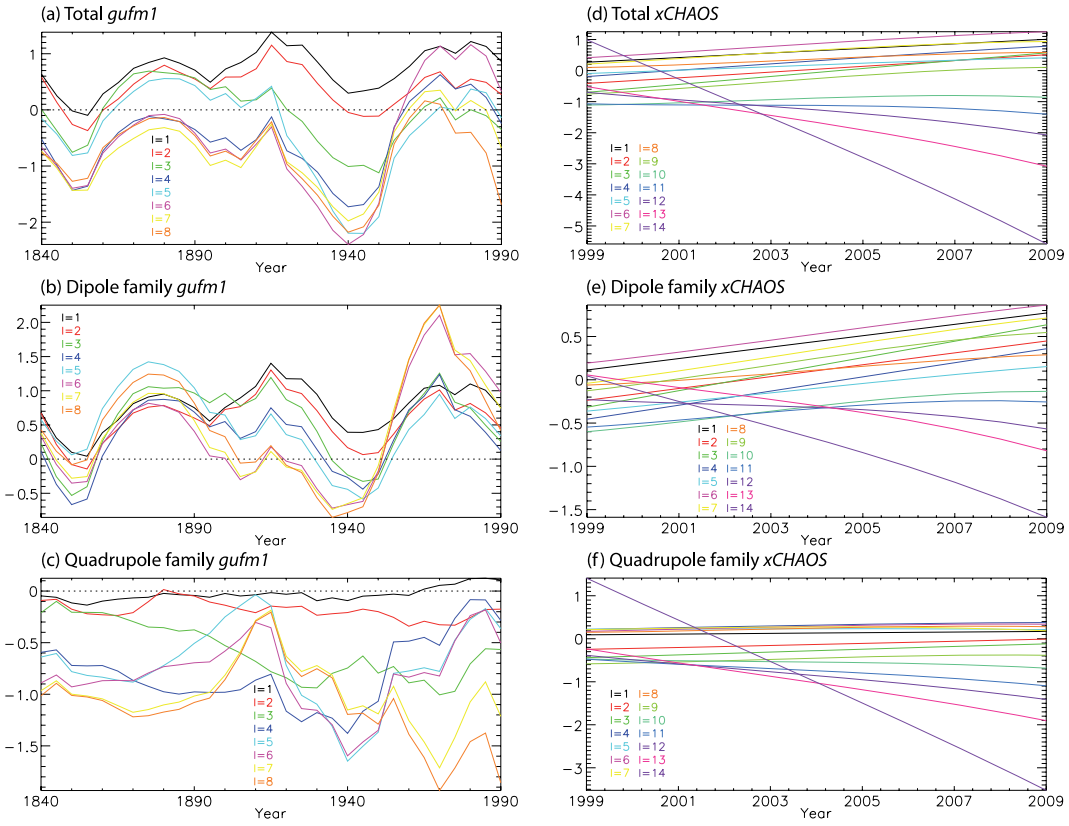

Figure 7. Flux spectra of the core field F_n in $\mathrm{nT}^2\,\mathrm{yr}^{-1}$ as a function of spherical harmonic degree n and time.

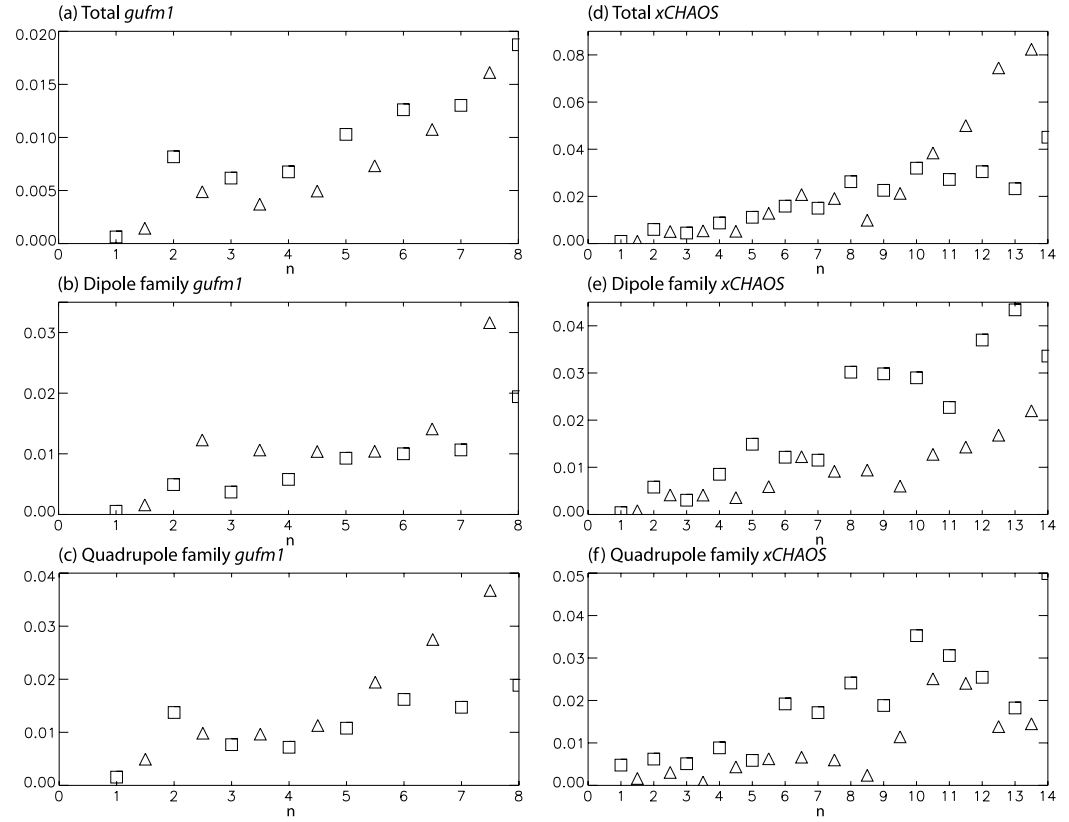

Figure 8. Time average of the absolute value of the spectral transfer rate γ_n (triangles) compared with time average of the SV rate $1/\tau_n$ (squares), both in yr^{-1}, versus spherical harmonic degree n, for core field models *gufm1* between 1840–1990 (a)-(c) and *xCHAOS* between 1999–2000 (d)-(f).

dynamo remains practically constant, the dipole intensity rapidly decreases while the non-dipole field compensates by increasing intensity.

Fig. 9 shows an example of magnetic energy cascade during a dipole collapse event from a numerical dynamo model. The control parameters of this model are Ekman number $E = 0.006$, Prandtl number $Pr = 1$, magnetic Prandtl number $Pm = 20$, and a compositional Rayleigh number Ra about 10 times supercritical, with no-slip mechanical boundary conditions, zero light element flux at the outer boundary, and fixed light element concentration at the inner core boundary (for parameter definitions and more details see Olson 2007). The choice of $Pr = 1$ can be justified by the Prandtl turbulence hypothesis, while the choice of large Pm is aimed to produce a large magnetic Reynolds number and a chaotic dynamo. Although the control parameters in this specific dynamo model are very far from being Earth-like, especially the large Ekman number, this model is suitable for our purposes because it has a dipole-dominated magnetic field during stable polarity periods, with rapid dipole collapse events that sometimes result in polarity reversals (Olson 2007; Olson *et al.* 2009), a combination that is hard to find in numerical dynamos (Kutzner & Christensen 2002). The dipole collapse event shown here culminated in a polarity excursion, in which the dipole became very weak for about one half of a free decay time then re-strengthened on return to its original polarity. Magnetic field variables in Fig. 9 are scaled by $(\rho\Omega/\sigma)^{1/2}$, where σ, ρ, Ω are electrical conductivity, density, and angular velocity of rotation, respectively, and time is scaled by the most fundamental (longest) dipole free decay time, starting from an arbitrarily selected time before the main dipole collapse. Over the whole time interval the average dipole decrease rate is just 1.5 times the dipole free decay rate, however over some shorter periods, equivalent to about 150 yr, the dipole decrease rate reaches 6.5 times dipole free decay

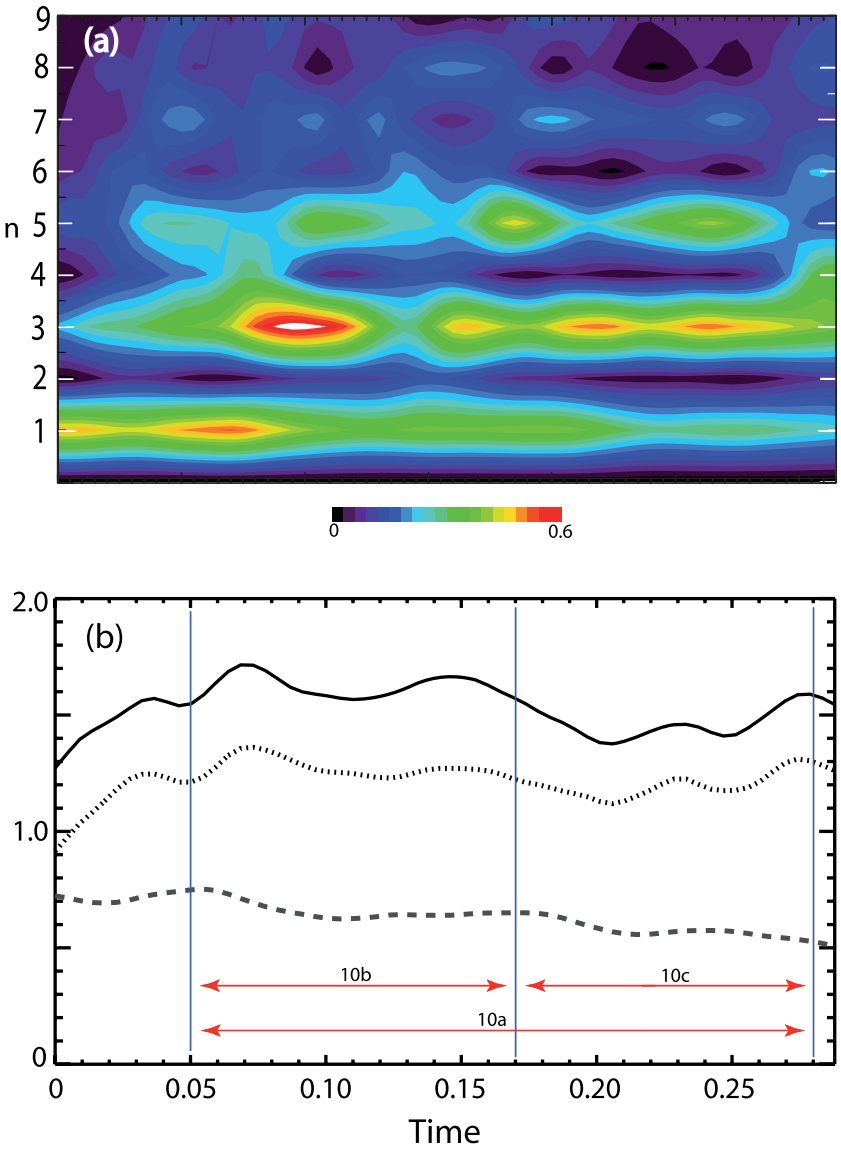

Figure 9. (a) The Mauersberger–Lowes spectrum of the total field at the outer boundary of the dynamo model as a function of time during a dipole decrease event. Spectral values are defined only at integer spherical harmonic degrees n. The linear-scale range of the dimensionless spectrum is given in the colour bar. (b) Time variation of the dimensionless rms total field intensity $B_{\rm rms}$ (solid), the rms non-dipole field intensity truncated at $n = 9$ $B_{\rm rms}(10 > n > 1)$ (dotted), and the rms dipole field intensity (dashed) $B_{\rm rms}(n = 1)$ on the outer boundary. Dimensionless time is in dipole free decay units. Blue vertical lines correspond to the three times indicated in Fig. 10, and the three periods are marked by the red arrow lines.

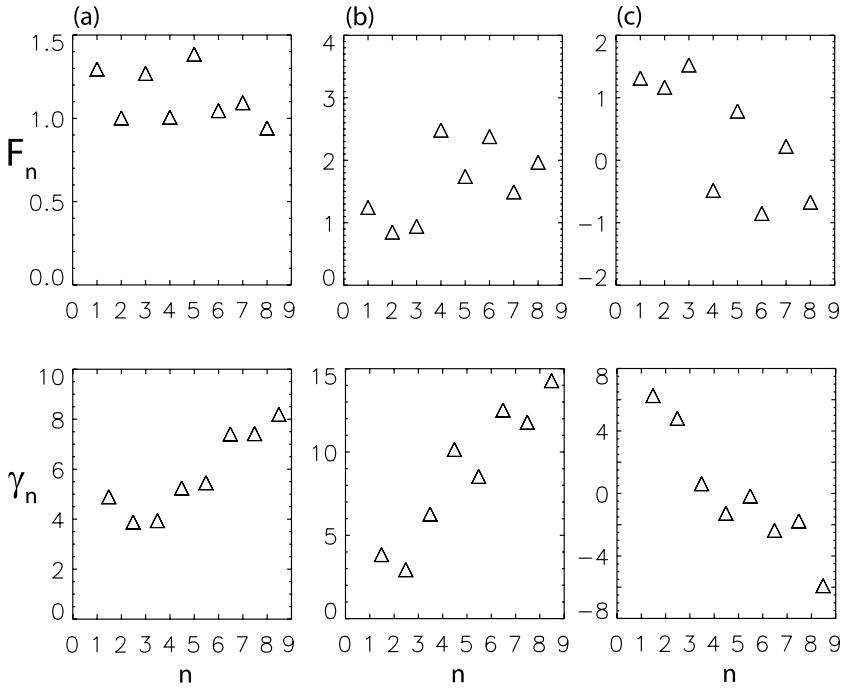

Figure 10. Time averages of dimensionless flux spectra F_n (top) and dimensionless spectral transfer rates γ_n (bottom) both scaled by the dipole free decay rate, versus spherical harmonic degree n during three time intervals of the dipole collapse event shown in Fig. 9. (a) time interval 0.05–0.28; (b) time interval 0.05–0.17; (c) time interval 0.17–0.28.

rate. For comparison, the present geomagnetic dipole decrease rate is about 11 times dipole free decay rate (Olson & Amit 2006).

Fig. 9(a) shows the variation of the Mauersberger–Lowes spectrum as a function of time at the outer boundary during the collapse. Although the model is taken to $n_{\max} = 32$, we consider only harmonics up to $n = 9$. Fig. 9(b) shows the variation of the total field intensity, the non-dipole intensity truncated at $n = 9$, and the dipole intensity, all at the outer boundary and non-dimensionalized with the same parameters as R_n. Over the time interval between 0.05 and 0.28 (which corresponds to about 4.5 kyrs for the core), the dipole intensity decreases substantially but the total field intensity net change from beginning to end is negligible. Meanwhile, the non-dipole intensity increases and magnetic energy in the Mauersberger–Lowes spectrum (Fig. 9a) appears at progressively higher harmonic degrees with time, as in an ideal forward cascade.

Fig. 10 shows time averages of the dimensionless flux spectrum F_n (top) and the dimensionless spectral transfer rate γ_n (bottom) over three time intervals from the dynamo model, calculated according to (20) and (22), respectively, using the dimensionless Mauersberger–Lowes spectrum R_n shown in Fig. 9 and values of D_n from the dynamo model. Fig. 10(a) corresponds to the time interval 0.05–0.28, which covers the main dipole collapse event. Fig. 10(b) corresponds to the time interval 0.05–0.17, while Fig. 10(c) corresponds to the time interval 0.17–0.28. Over each of these time intervals the net change in total field intensity is negligible, and as expected, the net effect of radial diffusion is also negligible.

Fig. 10(a) shows that, on average the flux spectrum F_n and the transfer rates γ_n are all positive and are of the same order of magnitude, corresponding to a nearly uniform, forward energy cascade throughout the low degree Mauersberger–Lowes spectrum. It is worth noting that the odd F_n are systematically larger than the even F_n, a consequence of $\dot{R}_n < 0$ for the odd whereas $\dot{R}_n > 0$ for the even harmonics. This behaviour may suggest that a quasi-local transfer in steps of two harmonics is significant in the evolution of the spectrum in this numerical dynamo model.

However, there are substantial short term variations in both F_n and γ_n within the collapse event, as the difference between Figs 10(b) and (c) reveals. Both of these sub-intervals begin with a dipole intensity fall, but in the first interval the non-dipole exhibits zero net intensity change, whereas in the second interval the non-dipole intensity has a net increase (see Fig. 9b). Fig. 10(b) shows that F_n and γ_n are larger than average and increase strongly with harmonic degree n when the dipole collapse is particularly rapid, consistent with the accelerated dipole decrease in a strong forward cascade during this time. In contrast, Fig. 10(c) shows that F_n and γ_n are small or negative and decrease with harmonic degree n, consistent with inverse cascade at high harmonics and energy trapping at intermediate harmonics during this time. It is perhaps unexpected that the cascade process is so strongly variable in time, even within a single dipole collapse event. In the next section, we show that comparable short-term variability is seen in the historical geomagnetic field.

5 GEOMAGNETIC DIPOLE INTENSITY STEPS

As noted before, in our local transfer model the spectral rate γ_n may be positive or negative, depending on whether the energy cascade is forward or inverse. During the historical era the dipole family is generally characterized by positive γ_n^a, corresponding to forward energy cascade from low to high harmonic degrees. In contrast, the quadrupole family exhibits negative γ_n^s and decreasing with n (Fig. 11, which is a signed version of Fig. 8c), corresponding to inverse energy cascade. The latter behaviour persists over the entire historical period, with only minor variations from one snapshot to another. It is perhaps counter-intuitive that γ_1^s is negative, suggesting

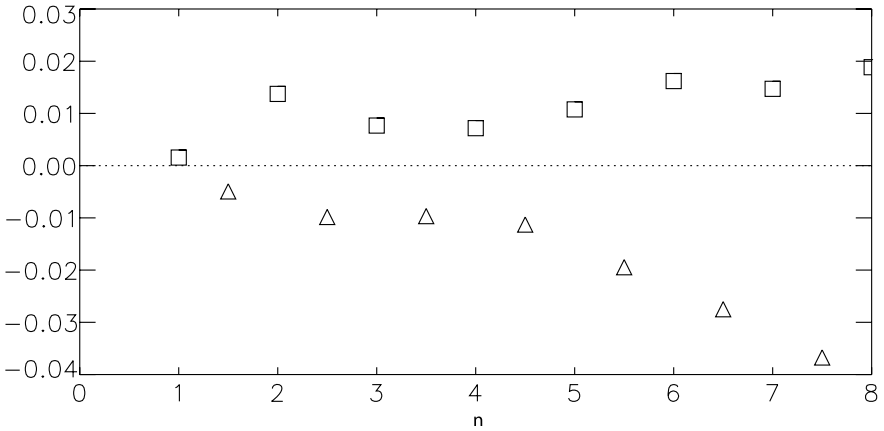

Figure 11. Time average (1840–1990) quadrupole family spectral transfer rate γ_n^s (triangles) compared with the corresponding SV rates $1/\tau_n^s$ (squares), both in yr^{-1}, versus spherical harmonic degree n, from core field model *gufm1*.

an energy flux to the equatorial dipole, despite the decrease in R_1^s over the historical period (Amit & Olson 2008). The reason is that over most of the historical period the equatorial dipole varies much more slowly compared to the other harmonics so free decay becomes comparable to and even larger than its SV, i.e. $|\dot{R}_1^s| < |D_1^s|$. Since 1960, however, the equatorial dipole decrease has accelerated, causing a poleward motion of the dipole tilt (Amit & Olson 2008), and in that period F_1^s became positive and large. The interpretation of the equatorial dipole time-evolution prior to 1960 in terms of our flux transfer method is therefore probably non-robust.

The numerical dynamo model results in the previous section demonstrate that γ_n may vary substantially over short time intervals within a longer dipole decrease event. Interpreted as a cascade process, changes in γ_n correspond to changes in the cascade direction, and can decelerate or accelerate a dipole decrease event. Evidence for these types of fluctuations can be seen in the historical core field. Fig. 12 shows the rms intensity of the dipole family B_{rms}^a on the CMB during the historical period. We focus on two time intervals, 1895–1935 labeled (a) when B_{rms}^a was nearly constant in time, and 1955–1990 labeled (b) when B_{rms}^a decreased precipitously. The time averages of the dipole family spectral transfer rates γ_n^a over these two intervals are shown in Fig. 13.

The transition from positive to negative γ_n^a with increasing n during 1895–1935 (Fig. 13a) is indicative of magnetic energy forward cascade from the dipole and magnetic energy inverse cascade from $n = 8$, resulting in magnetic energy trapping at intermediate harmonic degrees. This is consistent with simultaneous axial dipole decrease and constant B_{rms}^a (Fig. 12) in which the energy cascading from the dipole remains within the observable part of the core field spectrum. Note the similarity between γ_n^a in Fig. 13(a) to the spectral transfer rate in the numerical dynamo dipole collapse during its slower stage (Fig. 10c). Similarly, the increase in γ_n^a with increasing n for 1955–1990 (Fig. 13b) indicates a forward energy cascade, which simultaneously accounts for the decrease of the axial dipole and the sharp decrease in B_{rms}^a (Fig. 12), allowing energy to leave the observable part of the core field spectrum via a uniformly forward cascade. Here again there is close resemblance to γ_n in the numerical dynamo during its time of most rapid dipole decrease (Fig. 10b).

Analysis of the high resolution satellite field model *xCHAOS* reveals that the difference among the individual F_n curves increases significantly within one decade, demonstrating the rapid changes in the geodynamo (Olsen & Mandea 2008). Comparing the large-scale spectral transfer rates for 1999–2009 (Fig. 8e) with the corresponding time average for the preceding period 1955–1990 (Fig. 13b) shows in both cases positive trends, suggesting forward cascade at low harmonic degrees, although at lower rates than in the historical field. The higher degrees revealed using the modern field

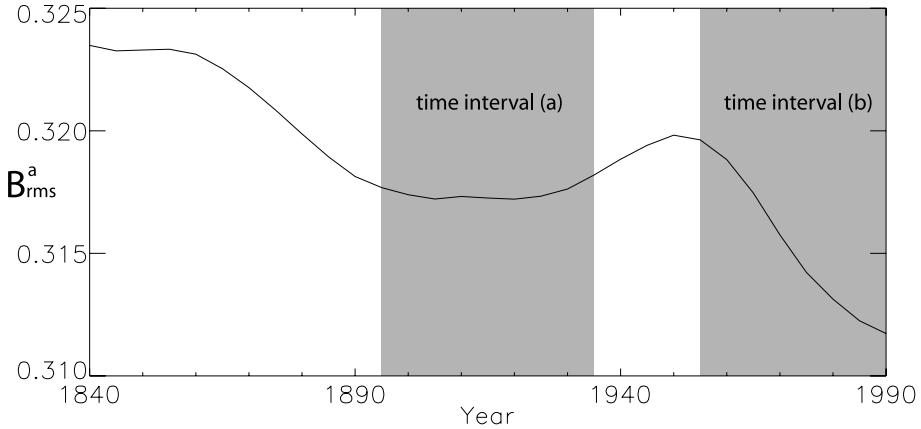

Figure 12. Dipole family rms intensity B_{rms}^a in mT for 1840–1990 from core field model *gufm1*. The two shaded time intervals (a) and (b) correspond to the time averages shown in Fig. 13.

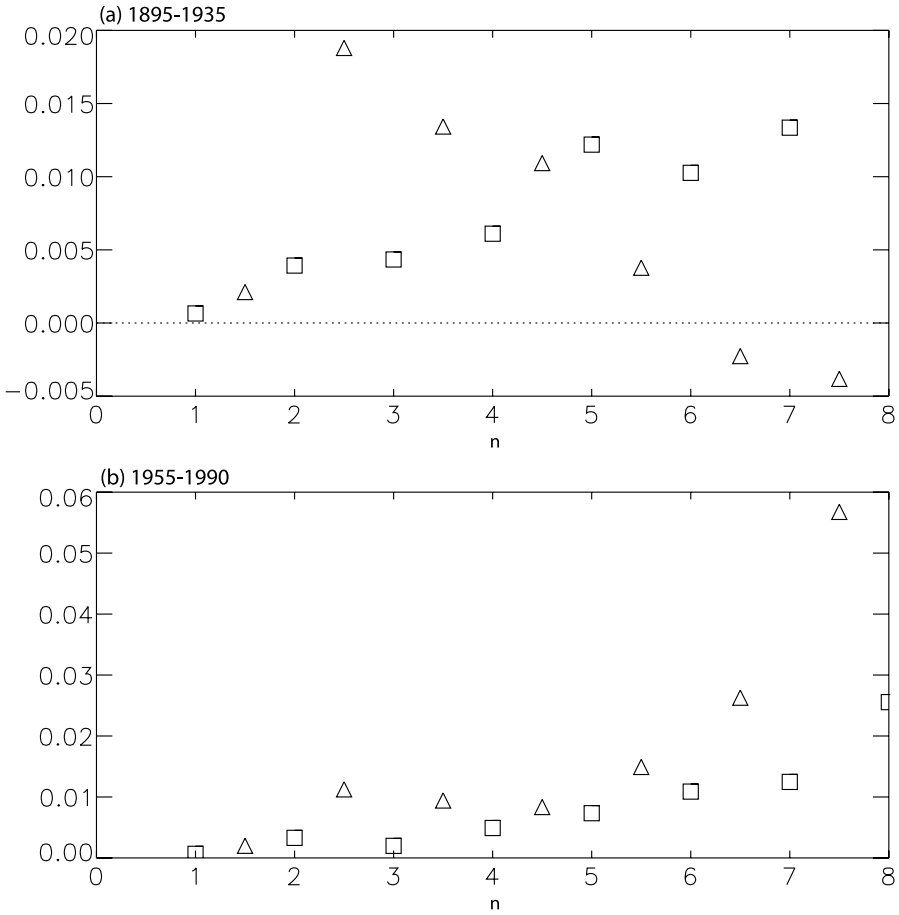

Figure 13. Dipole family spectral transfer rates γ_n^a (triangles) compared with corresponding SV rates $1/\tau_n^a$ (squares), both in yr^{-1}, versus spherical harmonic degree n averaged over the two time intervals (a) 1895–1935; and (b) 1955–1990, shown in Fig. 12.

model *xCHAOS* exhibit negative γ_n^a at higher harmonic degrees (not shown), suggesting that magnetic energy is trapped at $n \sim 9$. For the quadrupole family, the monotonic decrease of γ_n^s with n during the historical era (Fig. 11) transforms into a more complicated n-dependence in the modern era (not shown), although for most degrees the rates are again negative, indicative of inverse magnetic energy cascade in the quadrupole family.

6 RELATION WITH PREVIOUS GEOMAGNETIC DIPOLE MOMENT ANALYSES

Core flow models inferred from inversions of geomagnetic SV data were used to study dipole moment variations. Most core flow models neglect magnetic diffusion, under the so-called frozen-flux approximation (Roberts & Scott 1965), assuming that the magnetic Reynolds number in the core is large. Olson & Amit (2006) introduced a new theory that combines core flow and magnetic field models to map the advective contributions to the axial dipole SV. According to their formulation, axial dipole moment advective sources and sinks form where meridional flow interacts with radial magnetic field. Applying their derivation for the geomagnetic field, they identified regions below the CMB where advection weakens the dipole moment. They concluded that the geomagnetic axial dipole moment decrease is caused by the combined effects of intensification and poleward migration of reversed dipolar field as well as normal dipolar field equatorward motion (see also Voorhies 1991). Amit & Olson (2008) applied the same theory to localize advective sources and sinks of equatorial dipole moment that are responsible for dipole tilt variations. They found that the recent dipole tilt decrease event in the past 40 yr is caused by two equatorial dipole advective sinks where positive/negative radial magnetic field is transported westward/northward towards/away from the negative equatorial pole, respectively.

In fact, the core flow models of Jackson (1997) systematically underestimate axial dipole SV, which he hypothesized is an artefact of the tangential geostrophy constraint. In contrast, Whaler & Davis (1997) argued that this underestimation is due to unmodelled effects of magnetic diffusion. Core flow models constructed assuming steady flow in a drifting reference frame (Voorhies & Backus 1985) were found to improve the fit to the axial dipole SV (Holme & Whaler 2001). Increasing evidence for magnetic diffusion motivated incorporation of diffusion effects in core flow inversion schemes. The difficulty of accounting for diffusion is that the variation of the field with depth is unknown, so radial diffusion SV cannot be imaged from observations. Voorhies (1993) argued that diffusive field expulsion and fluid upwelling will have the same kinematic effect in terms of the observed SV. Holme & Olsen (2006) estimated diffusive SV using free decay modes. Their largest estimates were assigned for the lowest degrees, most notably the dipole. These free decay models were used as error estimates in their core flow inversions. Surprisingly, the resulting flows were nearly unchanged compared to the flows inverted using conventional error estimates,

perhaps indicating that the flows cannot account for diffusive effects (Holme 2007). A different approach was taken by Amit & Christensen (2008). They found in numerical dynamos that radial and tangential diffusion effects are well-correlated. They then used the pattern of tangential diffusion from observations and an extrapolated magnitude to account for radial diffusion in order to model full magnetic diffusion. Comparison of their diffusive and frozen-flux inverted core flows suggests that accounting for radial magnetic diffusion may in some locations affect significantly images of the flow at the top of Earth's core.

Our cascade model may be viewed as a complimentary approach to core flow inversions. Our calculated transfer rates cannot substitute for core flow models; these rates provide only a 1-D description of magnetic field advection in spectral space, while core flows provide a 2-D image on the CMB. However, the process of core flow inversions suffer from numerous assumptions, making the results of theses models open to diverse interpretations (for a review see Holme 2007). Our study may provide a framework for testing inverted core flow models. By substituting a spectral description of the velocity field at the top of the core into (9) the transfer spectrum T_n is found, from which the spectral flux F_n can be calculated (19), and finally the spectral transfer rate γ_n is obtained using (22). Comparison of γ_n inferred from an inverted core flow model with our direct calculation from the Mauersberger–Lowes spectra may connect inverted core flow models with the Mauersberger–Lowes spectra and highlight the ability of these models to capture the spectral transfer phenomenon in general, and the dipole decrease in particular. Such a comparison, though beyond the scope of this study, is a worth-while future prospect.

7 CONCLUDING REMARKS

We interpret the changes in the low degree Mauersberger–Lowes geomagnetic spectrum at the CMB since 1840 using a magnetic energy cascade model. Our model is motivated by the simultaneous dipole field decrease and the non-dipole field increase over the past 170 yr. We quantify the evolution of the Mauersberger–Lowes spectrum by the spectral transfer rate γ_n, which indicates the rates of energy transfer between neighbouring spherical harmonic degrees. In our local transfer model, positive γ_n corresponds to forward cascade of energy through the spectrum (from n to $n+1$), negative γ_n corresponds to inverse energy cascade (from $n+1$ to n).

The values of our inferred spectral transfer rates are generally consistent with the traditional SV rates $1/\tau_n$, and also consistent with the independently estimated geodynamo memory time (Hulot *et al.* 2010). However, we find that the transfer rates themselves fluctuate significantly, sometimes changing sign, particularly within the dipole family. Between 1955 and 1990 for example, the rms dipole family intensity $B^a_{\rm rms}$ decreases rapidly and γ^a_n increases with n, implying a forward cascade with energy transfer out of the core field spectrum towards $n > 8$. In contrast, between 1895–1935 $B^a_{\rm rms}$ is nearly constant while γ^a_n decreases with n, becoming negative at $n > 6$, implying energy trapping at intermediate n-values in the core field spectrum. A numerical dynamo model shows comparable behaviour during a prolonged dipole decrease event. For the geomagnetic quadrupole family, we find γ^s_n is negative and decreases with n, suggesting an inverse cascade.

In spite of these general similarities to a cascade process, we acknowledge that caution should be exercised in applying this model to the geomagnetic field. The central assumption of our model, local transfer through the magnetic energy spectrum, is not a universal property in MHD systems. Our free decay model of magnetic diffusion serves as an energy sink only, while diffusive sources in the form of magnetic field expulsion are not modelled. In addition, there is conflicting evidence in the geomagnetic field behaviour (see Fig. 7 and its discussion in Section 3).

Our analytical examples show that our model can capture the cascade phenomenon provided that local energy transfer is dominant, but it can equally interpret non-local transfer as local. Although we point to some geomagnetic examples (e.g. Figs 2–5), further identification of local spectral transfer in core field is needed, in order to substantiate our model. Extended, high resolution records of the core field expected from future satellite missions such as SWARM could make this possible.

Finally we address the important issue of whether the current geomagnetic dipole decrease will result in a reversal. The similarity between the forward energy cascade in the dipole collapse event that preceded a reversal in the numerical dynamo model and the forward energy cascade in the dipole family of the geomagnetic field may be viewed as evidence for a beginning of a reversal. However, we have shown that the time-variability of the spectral transfer rates is very strong. It is therefore probably impossible to know, based on the relatively short 150-yr period of available high resolution geomagnetic field observations, whether these cascade trends will prevail and lead to a reversal or not. Improvement in the quality and spatial resolution of archaeomagnetic field models may allow examining the persistence of the forward cascade trends inferred from the historical field over millennial timescales.

ACKNOWLEDGMENTS

We thank F.J. Lowes and C.V. Voorhies for their very detailed reviews that significantly improved the manuscript. We also thank R. Holme for his useful comments. PO gratefully acknowledges support from NSF Geophysics Grant EAR0604974.

REFERENCES

Alexakis, A., Mininni, P. & Pouquet, A., 2005. Imprint of large-scale flows on turbulence, *Phys. Rev. Lett.,* **93,** 264503.

Alexakis, A., Mininni, P. & Pouquet, A., 2007. Turbulent cascades, transfer, and scale interactions in magnetohydrodynamics, *New J. Phys.,* **9,** 1–20.

Alldredge, L., 1984. Harmonics required in main field and secular varaition models, *J. Geomagn. Geoelectr.,* **36,** 63–72.

Amit, H. & Christensen, U., 2008. Accounting for magnetic diffusion in core flow inversions from geomagnetic secular variation, *Geophys. J. Int.,* **175,** 913–924.

Amit, H. & Olson, P., 2006. Time-average and time-dependent parts of core flow, *Phys. Earth planet. Inter.,* **155,** 120–139.

Amit, H. & Olson, P., 2008. Geomagnetic dipole tilt changes induced by core flow, *Phys. Earth planet. Inter.,* **166,** 226–238.

Backus, G., Parker, R. & Constable, C., 1996. *Foundations of Geomagnetism*, Cambridge University Press, Cambridge, UK.

Benton, E. & Alldredge, L., 1987. On the interpretation of the geomagnetic energy spectrum, *Phys. Earth planet. Inter.,* **48,** 265–278.

Benton, E. & Voorhies, C., 1987. Testing recent geomagnetic field models via magnetic flux conservation at the core-mantle boundary, *Phys. Earth planet. Inter.,* **48,** 350–357.

Biskamp, D., 2003. *Magnetohydrodynamic Turbulence*, Cambridge University Press, Cambridge, UK.

Bloxham, J., 1986. The expulsion of magnetic flux from the Earth's core, *Geophys. J. R. astr. Soc.,* **87,** 669–678.

Bloxham, J. & Jackson, A., 1991. Fluid flow near the surface of the Earth's outer core, *Rev. Geophys.,* **29,** 97–120.

Boldyrev, S., 2006. Spectrum of magnetohydrodynamic turbulence, *Phys. Rev. Lett.,* **96,** 115002.

Cain, J., Wang, Z., Schmitz, D. & Meyer, J., 1989. The geomagnetic spectrum for 1989 and core-crustal separation, *Geophys. J.,* **97,** 443–447.

Cho, J., Lazarian, A. & Vishniac, E., 2002. Simulations of magnetohydrodynamic turbulence in a strongly magnetized medium, *Astr. J.,* **564,** 291–301.

Christensen, U. & Tilgner, A., 2004. Power requirement of the geodynamo from ohmic losses in numerical and laboratory dynamos, *Nature,* **439,** 169–171.

Corrsin, S., 1961. The reactant concentration spectrum in turbulent mixing with a first-order reaction, *J. Fluid Mech.,* **11,** 407–416.

Corrsin, S., 1964. Further generalization of Onsager's cascade model for turbulent spectra, *Phys. Fluids,* **7,** 1156–1159.

Dormy, E., Valet, J.-P. & Courtillot, V., 2000. Numerical models of the geodynamo and observational constraints, *Geochem. Geophys. Geosyst.,* **1**(10), 1037, doi:10.1029/2000GC000062.

Eymin, C. & Hulot, G., 2005. On surface core flows inferred from satellite magnetic data, *Phys. Earth planet. Inter.,* **152,** 200–220.

Finlay, C., 2008. Historical variation of the geomagnetic axial dipole, *Phys. Earth planet. Inter.,* **170,** 1–14.

Frisch, U., 1995. *Turbulence: The Legacy of A.N. Kolmogorov*, Cambridge University Press, Cambridge, UK.

Gillet, N., Pais, M. & Jault, D., 2009. Ensmeble inversion of time-dependent core flow models, *Geochem. Geophys. Geosyst.,* **10,** Q06004.

Gubbins, D., 1987. Mechanism for geomagnetic polarity reversals, *Nature,* **326,** 167–169.

Gubbins, D., Jones, A. & Finlay, C., 2006. Fall in Earth's magnetic field is erratic, *Science,* **312,** 900–902.

Hill, R., 1978. Models of the scalar spectrum for turbulent advection, *J. Fluid Mech.,* **88,** 541–562.

Holme, R., 2007. Large-scale flow in the core, in *Treatise on Geophysics*, Vol. 8. ed. Olson, P., Elsevier Science, London.

Holme, R. & Olsen, N., 2006. Core surface flow modelling from high-resolution secular variation, *Geophys, J. Int.,* **166,** 518–528.

Holme, R. & Whaler, K., 2001. Steady core flow in an azimuthally drifting frame, *Geophys. J. Int.,* **145,** 560–569.

Hongre, L., Hulot, G. & Khokhlov, A., 1998. An analysis of the geomagnetic field over the past 2000 years, *Phys. Earth planet. Inter.,* **106,** 311–335.

Hulot, G. & LeMouël, J.-L., 1994. A statistical approach to the Earth's main magnetic field, *Phys. Earth planet. Inter.,* **82,** 167–183.

Hulot, G., Lhuillier, F. & Aubert, J., Earth's dynamo limit of predictability, *Geophys. Res. Lett.,* **37,** L06305, doi:10.1029/2009GL041869.

Jackson, A., 1997. Time-dependency of tangentially geostrophic core surface motions, *Phys. Earth Planet. Inter.,* **103,** 293–311.

Jackson, A., Jonkers, A. & Walker, M., 2000. Four centuries of geomagnetic secular variation from historical records, *Phil. Trans. R. Soc. Lond. A,* **358,** 957–990.

Korte, M. & Constable, C., 2005. Continuous geomagnetic field models for the past 7 millennia: 2. CALS7K, *Geochem. Geophys. Geosyst.,* **6**(2), doi:10.1029/2004GC000801.

Kutzner, C. & Christensen, U., 2002. From stable dipolar towards reversing numerical dynamos, *Phys. Earth planet. Inter.,* **131,** 29–45.

Liu, L. & Olson, P., 2009. Geomagnetic dipole moment collapse by convective mixing in the core, *Geophys. Res. Lett.,* **36,** L10305, doi:10.1029/2009GL038130.

Lowes, F., 1974. Spatial power spectrum of the main geomagnetic field, *Geophys. J. R. astr. Soc.,* **36,** 717–730.

Maron, J. & Goldreich, P., 2001. Simulations of incompressible magnetohydrodynamic turbulence, *Astr. J.,* **554,** 1175–1196.

McLeod, M., 1996. Spatial and temporal power spectra of the geomagnetic field, *J. geophys. Res.,* **101,** 2745–2764.

Moffatt, H., 1978. *Magnetic Field Generation in Electrically Conducting Fluids*, Cambridge University Press, Cambridge, UK.

Müller, W. & Grappin, R., 2005. Spectral energy dynamics in magnetohydrodynamic turbulence, *Phys. Rev. Lett.,* **95,** 114502.

Olsen, N. & Mandea, M., 2008. Rapidly changing flows in the Earth's core, *Nat. Geosci.,* **1,** 390–394.

Olson, P., 2007. Gravitational dynamos and the low frequency geomagnetic secular variation, *Proc. Natl. Acad. Sci. U.S.A.,* **104,** 20 159–20 166.

Olson, P. & Amit, H., 2006. Changes in earth's dipole, *Naturwissenschaften,* **93,** 519–542.

Olson, P., Driscoll, P. & Amit, H., 2009. Dipole collapse and reversal precursors in a numerical dynamo, *Phys. Earth planet. Inter.,* **173,** 121–140.

Pais, M.A. & Jault, D., 2008. Quasi-geostrophic flows responsible for the secular variation of the Earth's magnetic field, *Geophys. J. Int.,* doi:10.1111/j.1365–246X.2008.03741.x.

Poirier, J.-P., 2000. *Introduction to the Physics of the Earth's Interior*, Cambridge University Press, Cambridge, UK.

Pouquet, A., Frisch, U. & Léeorat, J., 1976. Strong MHD helical turbulence and the nonlinear dynamo effect, *J. Fluid Mech.,* **77,** 321–354.

Roberts, P., 1971. Dynamo theory, in *Mathematical Problems in the Geophysical Sciences*, ed. Reid, W., Amer. Math. Soc., Providence, Rhode Island.

Roberts, P. & Scott, S., 1965. On analysis of the secular variation, 1, a hydromagnetic constraint: theory, *J. Geomagn. Geoelectr.,* **17,** 137–151.

Verosub, K. & Cox, A., 1971. Changes in the total magnetic energy external to the Earth's core, *J. Geomagn. Geoelectr.,* **23,** 235–242.

Voorhies, C., 1991. Coupling an inviscid core to an electrically insulating mantle, *J. Geomagn. Geoelectr.,* **43,** 131–156.

Voorhies, C., 1993. Geomagnetic estimates of steady surficial core flow and flux diffusion: unexpected geodynamo experiments, in *Dynamics of Earth's deep interior and Earth rotation*, Vol. 12. eds LeMouël, J.-L., Smylie, D. & Herring, T., Geophysical Monograph 72 IUGG.

Voorhies, C., 2004. Narrow-scale flow and a weak field by the top of Earth's core: evidence from Orsted, Magsat, and secular variation, *J. geophys. Res.,* **109,** doi:10.1029/2003JB002833.

Voorhies, C. & Backus, G., 1985. Steady flows at the top of the core from geomagnetic field models - the steady motions theorem, *Geophys. Astrophys. Fluid Dyn.,* **32,** 163–173.

Whaler, K. & Davis, R., 1997. Probing the Earth's core with geomagnetism, in *Earth's Deep Interior*, ed. Crossley, D., Gordon and Breach, Amsterdam, the Netherlands.

Wiltse, J. & Glezer, A., 1993. Manipulation of free shear flows using piezoelectric actuators, *J. Fluid Mech.,* **249,** 261–285.

Yousef, T., Rincon, F. & Schekochihin, A., 2007. Exact scaling laws and the local structure of isotropic magnetohydrosdynamic turbulence, *J. Fluid Mech.,* **575,** 111–120.